Chapter – 2

Materials and Methods

CHAPTER 2: Materials and Methods

2.1 Overview

In order to accomplish the goals described in Chapter 1, it is crucial to synthesize and identify the proposed systems to analyze their properties and potential uses. This chapter encompasses the specific synthesis techniques, characterization utilizing different tools, and relevant experimental approaches to assess the diverse qualities of the proposed systems. The materials proposed in this study include (a) CuO/Cu_2O thin films, (b) CuO nanoparticles, (c) $Cu_{1-x}Ni_xO$ (x = 0, 0.2, 0.4, 0.6, 0.8, and 1) composite. The CuO/Cu_2O thin films were fabricated on a Silicon (Si) substrate by the Pulsed Laser Deposition (PLD) technique, CuO nanoparticles were synthesized by hydrothermal method, and the composite system listed in (c) was synthesized by solid-state reaction (SSR) method. The prepared samples underwent analysis to assess their structural, optical, microstructural, thermal, and photoelectrochemical properties. This chapter is divided into three sections. The first part focuses on the preparation and processing of the compositions. The subsequent section outlines the various methods of characterization utilized in this study. The final section delves into the different techniques for analyzing the data.

2.2 Specification of the Materials

Raw materials of high purity were used for the synthesis of photocathodes. The details of the materials, including their purity, chemical formula, and manufacturer, are outlined in Table 2.1.

Table 2.1: Details of the raw materials

S. No	Raw Materials	Chemical Formula	Purity	Manufacturer
1.	Cupric oxide	CuO	99.9%	Merck
2.	Cupric nitrate trihydrate	$Cu(NO_3)_2 * 3H_2O$	> 99%	Thermo fisher scientific
3.	Nickel oxide	NiO	99%	Alfa Aesar

Moreover, the compounds were also fabricated using various reagents, chemicals, and solvents such as sodium hydroxide (NaOH), ethanol, isopropanol, and acetone.

2.3 Synthesis of Materials

Pulsed Laser Deposition (PLD) was employed to process the material and create thin films. Nanoparticles were synthesized through a versatile hydrothermal method. The SSR method was used to synthesize the bulk composite materials. Further elaboration on these synthesis techniques is discussed in the following section, which is used in the present investigation.

2.3.1 Solid State Reaction (SSR) Method

The solid-state reaction route (SSR), often known as the ceramic method, involves a chemical process that creates a new solid with a well-defined structure using solid starting materials. Some metal oxides or salts do not react with each other at room temperature, so extreme conditions such as high temperature and pressure are required to induce the reaction. Before weighing, the reactants are dried. Once the necessary amount is measured, they are meticulously mixed using an agate mortar and pestle (manual mixing) with acetone to assist

in homogenization. The acetone evaporation takes typically 10-20 minutes after the mixing and grinding. To achieve the desired result, repeat this process 3 to 4 times. This technique is also called "heat and beat" or "shake and bake". The rate of reaction in SSR methods is affected by various factors such as the shape and surface area of reactants, reaction conditions, structural properties of the reactants, their reactivity, thermodynamic properties of nucleation, and diffusion rate. Figure 2.1 shows the schematic diagram of the SSR method. There are several advantages of this synthesis technique, as outlined below:

1) High-purity product.
2) Simplicity in handling and processing.
3) Increased productivity.
4) Control over composition
5) Simple and cost-effective process

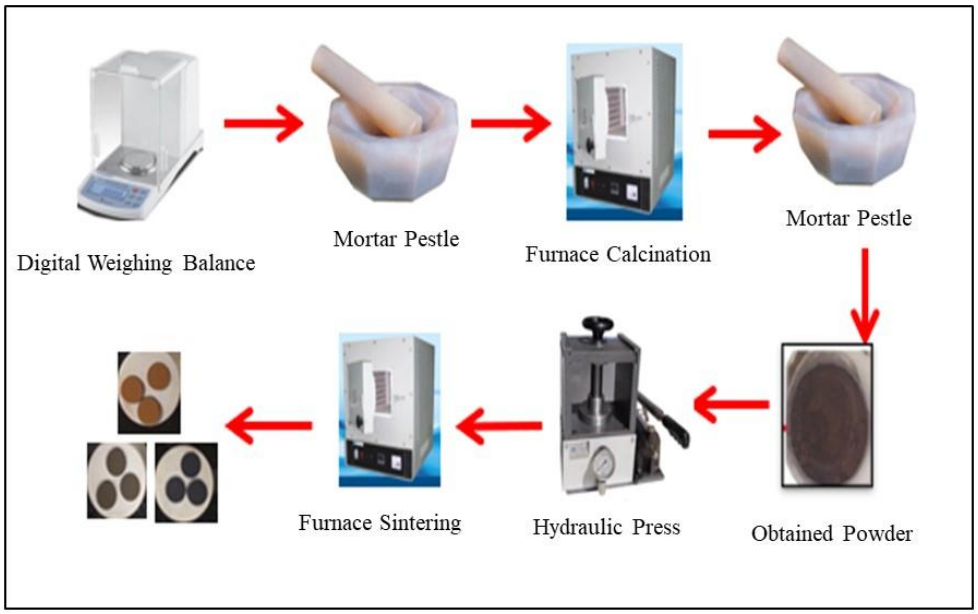

Figure 2.1: Schematic diagram of the solid-state route (SSR) method.

2.3.2 Pulsed Laser Deposition (PLD) Technique

The process of PLD involves a straightforward method for depositing thin films. This technique uses a high-power pulsed laser beam to provide an external energy source to hit the target material. The setup comprises a vacuum chamber housing both target and substrate holders. Laser sources like XeCl (308 nm), KrF (248 nm), and Nd-YAG laser are currently used for material ablation. The pulsed laser beam is at a 45° angle toward the target holder. When the target material absorbs the laser beam, it generates a colourful plasma plume on the material's surface, consisting of electrons, atoms, ions, and molecules. The substance extracted from this process is then steadily deposited onto the substrate, forming a uniform film. The deposition process is carried out in a vacuum or a low-gas-pressure environment. Numerous experimental conditions can be altered during deposition, significantly impacting the film's properties. When dealing with multi-element materials, PLD is often more convenient for achieving the required film stoichiometry than other deposition processes. In this thesis work, the thin films were deposited on a Si substrate using PLD [63], and an image of the PLD setup is shown in Fig. 2.2.

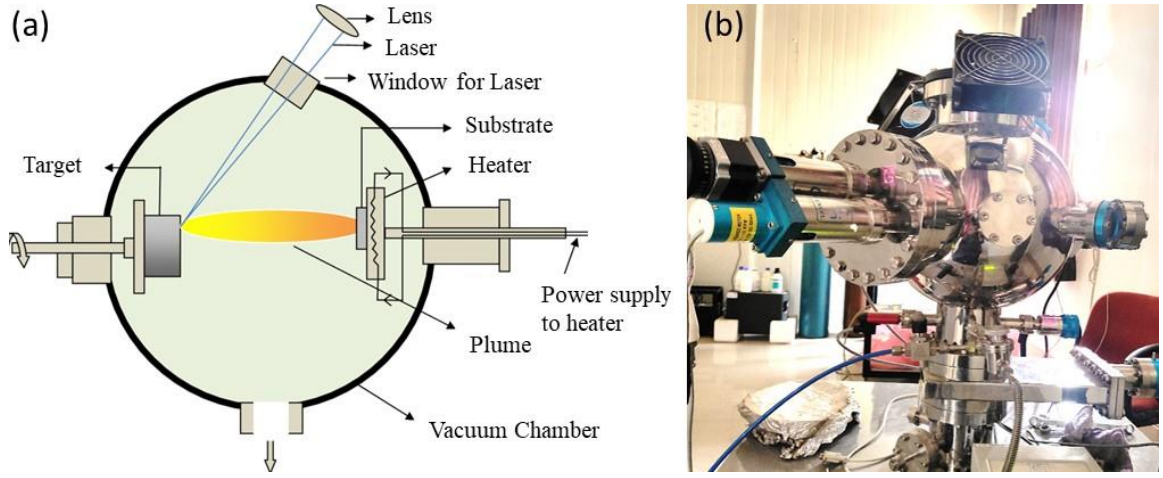

Figure 2.2: Schematic diagram of pulse laser deposition technique [64], (b) PLD facility at IIT (BHU).

The deposition process comprises four primary steps, which can be explained as follows:

1) Applying laser energy to absorb onto the target surface leads to laser ablation of the target material and plasma creation.
2) Management of plasma dynamics.
3) The ablated material deposits onto the substrate.
4) Film nucleation begins on the substrate and continues with its growth.

PLD offers several advantages, including:

1) High deposition rate.
2) Versatility in material deposition.
3) Control on film thickness.
4) Stoichiometric transfer.
5) Multi-layer deposition with low contamination.

2.3.3 Hydrothermal Method

The hydrothermal method is a versatile and effective technique for creating high-quality crystals and advanced materials. In the typical synthesis process, a precursor material is dissolved in water or another solvent, then heated and pressurized in a sealed autoclave. High temperature and high-pressure conditions help the material crystallize from the solution. This method precisely manipulates the resulting crystal's size, shape, and structure, which is especially valuable for producing materials with particular properties.

Some advantages of the hydrothermal method are:

1) Achieving high-purity crystals.

2) Low operating temperatures compared to other synthesis techniques.
3) Controlled crystallization.
4) Versatile method

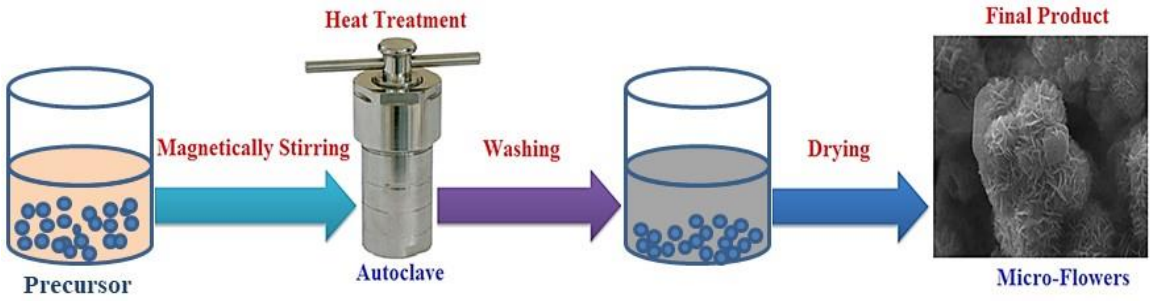

Figure 2.3: Schematic diagram of hydrothermal synthesis method [65].

2.4 Characterization Techniques

2.4.1 X-ray diffraction (XRD)

XRD is a highly effective and non-invasive technique for analyzing crystalline materials, and it can potentially provide valuable characterization. Its application includes identifying material type and phase and determining preferred orientation and other structural parameters such as crystallinity, average grain size, and crystal defect. The main components of an X-ray diffractometer include an X-ray source, a sample stage, and a detector for X-rays.

Working principle:

This analytical technique relies on the scattering of X-rays by material. Copper (Cu) is the most frequently used material for single-crystal diffraction, and the analysis utilizes an X-ray source that emits Cu Kα radiation (λ= 1.5406 Å). X-rays are generated in a cathode ray tube by heating a filament to generate electrons. Subsequently, a voltage is applied to accelerate the electrons

towards a target, bombarding the target material with electrons. The sample is placed in a diffractometer at the center of the instrument and exposed to the X-ray beams. The movement of the X-ray tube and detector is synchronized. The measurement of the distance between atoms uses a unique interference effect called "diffraction" because the wavelength of X-rays is similar to the spacing between a crystal's atoms. Bragg's diffraction is the predominant type of diffraction used in X-ray crystallography. When incident X-rays interact with the electrons of the atoms, they are scattered, a phenomenon known as elastic scattering, where the scatterer is the electron. A regular array of scatterers produces spherical waves. Although destructive interference causes these waves to cancel out in most directions, they align constructively in specific directions following Bragg's law [66]. Bragg's law defines the condition for constructive diffraction by the following equation:

$$2d \sin\theta = n\lambda \tag{2.1}$$

where d denotes the distance between the lattice plane, θ represents the angle of the diffracted wave, and n is the diffraction order. If the incident X-rays hit the sample in a way that satisfies the Bragg Equation, it results in constructive interference, producing a distinct peak. The signal from the sample is recorded and plotted, and a peak that matches the sample's atomic structure can be seen. Further, the crystallite size (D) of the samples can be determined by using the Debye - Scherer relation [67] by estimating the FWHM (β) from the XRD peaks, which is given by:

$$D = \frac{K\lambda}{\beta \cos\theta} \tag{2.2}$$

where, K is the Scherer constant, and λ represents the wavelength of the incident X-ray.

The most frequent use of X-ray diffraction is to identify unfamiliar crystalline materials. Another use is to measure a sample's purity and establish the unit cell's dimensions. XRD can also ascertain the crystal structure through the specialized technique known as 'Rietveld Refinement. Further details about Rietveld refinement will be covered later in this chapter. In this thesis, XRD is conducted using the (RIGAKU Miniflex, Japan) model to study the synthesized material (shown in Fig. 2.4(b)).

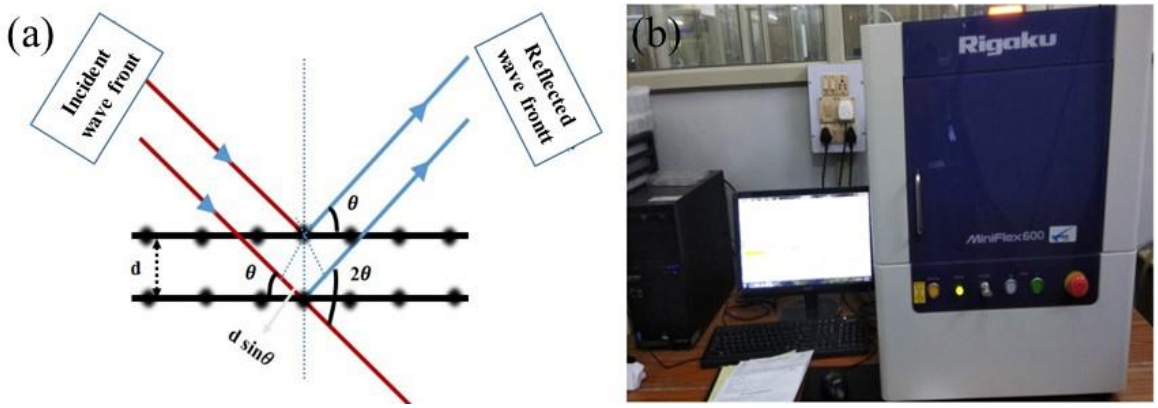

Figure 2.4: (a) Schematic representation of Bragg's law and its mechanism (b) Experimental setup of X-ray diffractometer at central instrumentation facility CIF IIT (BHU).

2.4.2 Thermogravimetric Analysis (TGA)

TGA is a technique used to determine the extent of change in mass of a sample over time or with respect to temperature in a controlled environment. Its purpose is to determine a substance's thermal stability and calcination temperature. If the mass of the sample remains constant within the specified temperature range, the sample is considered to be thermally stable at that temperature range.

Working principle:

The TGA comprises a precision balance and a sample pan, both crucial components. During the experiment, the sample pan is heated or cooled in a furnace, and the mass of the sample is measured continuously. The sample environment is managed by a sample purge gas, which passes through the sample and is released through an exhaust. This gas can either be reactive or inert. The primary components of a TGA apparatus include a high-precision thermobalance, a temperature-programmable furnace, and a facility for creating either an inert atmosphere or an oxidizing environment. In TGA, when a solid reactant is heated, it produces a product and emits gas, decreasing mass or weight. This decrease in mass may be due to gas formation from the reaction between the reactants under heat, or it may be caused by the presence of water in the reactants. The weight loss can be estimated by:

$$\text{Weight loss } (\Delta M) = m_{initial} - m_{final}$$

$$\text{Weight loss } \% = \left(\frac{\Delta M}{m_{initial}}\right) \times 100 \qquad (2.3)$$

where $m_{initial}$ is initial mass, m_{final} is final mass. The results of a thermogravimetric run can be presented as either weight versus temperature or weight loss versus temperature, resulting in a graph known as a thermogram. A plateau in the thermogram curve indicates no change in weight, while the curved portion suggests weight loss. The curve of measured weight loss provides information on kinetic parameters, thermal stability, and changes in sample compositions. The slope of the weight loss graph can reveal when weight loss becomes more apparent. Additionally, TGA can offer data on processes such as second-order transitions, vaporization, absorption, adsorption, oxidation, and reduction [68].

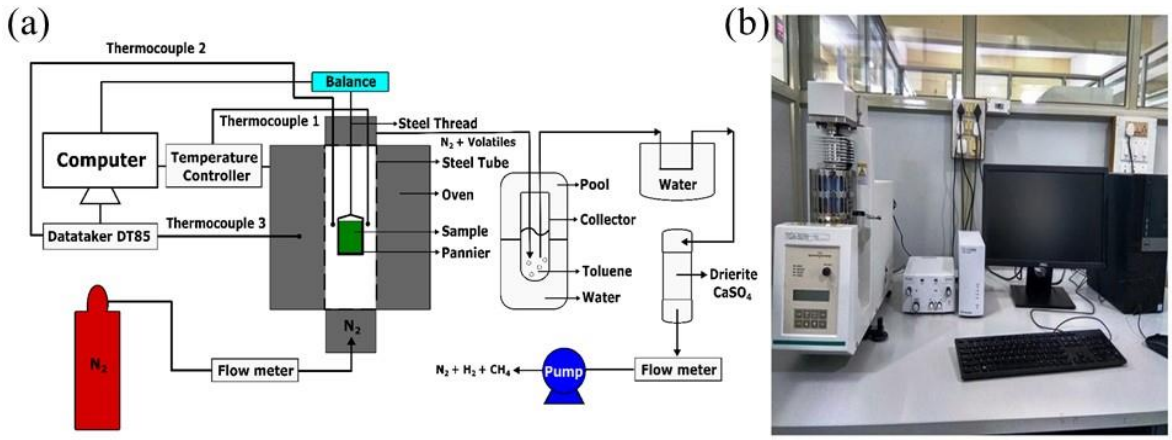

Figure 2.5: (a) Schematic representation of TGA [69] (b) Experimental setup of TGA at CIF IIT (BHU).

In this thesis work, TGA measurements were performed using the SHIMADZU TGA-50, as shown in Fig. 2.5(b).

2.4.3 Differential Scanning Calorimetry (DSC)

Differential scanning calorimetry (DSC) involves measuring the difference in heat transfer rates between a sample and a reference sample while both are subjected to a controlled temperature program. DSC is typically capable of accurately determining reaction and transition heats and monitoring heat flow rates and variations for small sample quantities over a broad temperature range. [70].

The two fundamental types of DSC are heat flux DSC and power compensation DSC. In heat flux DSC, the heat that is to be measured is transferred to the environment through a precisely defined heat conduction pathway with a set thermal resistance. In power compensation DSC, the heat detected is almost entirely counterbalanced by electrical energy through the adjustment of Joule heating. Both types of DSC have in common that, unlike most conventional calorimeters, the measured signal is proportional to a heat flow rate (ϕ) rather than a heat. Time

dependences of a transition can be found using the ϕ(t) curve. Due to this feature, all DSCs may handle challenges in various applications (directly measured heat flow rates).

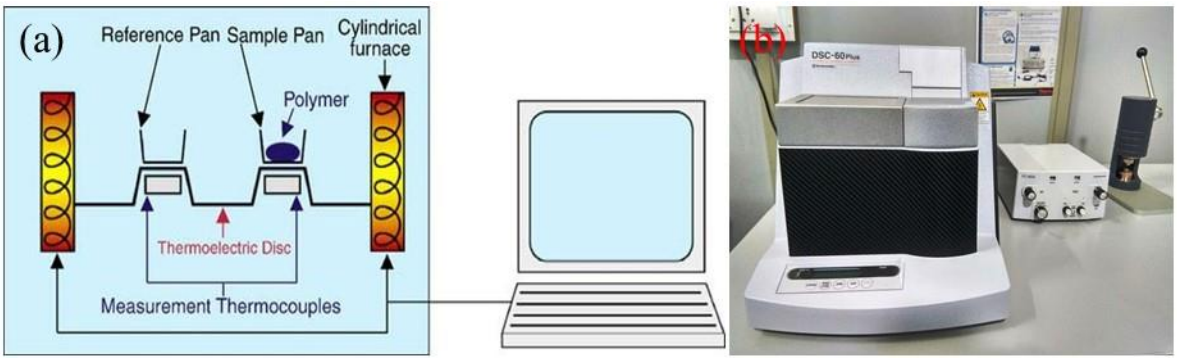

Figure 2.6: (a) Schematic representation of the mechanism of DSC [71] (b) Experimental setup of DSC at CIF IIT (BHU).

Working principle:

The DSC observes the heat flow difference between a sample and a reference material while they undergo controlled heating or cooling. Any endothermic or exothermic occurrences in the sample, such as melting or crystallization, lead to changes in heat flow that the DSC records. This data is essential for comprehending the thermal properties of the materials, including the glass transition process, phase transition, and heat capacity, and it offers valuable insights for material analysis. In the present thesis, DSC measurement was performed by SHIMADZU DSC-60 plus 230V, as shown in Fig. 2.6(b).

2.4.4 Scanning Electron Microscopy (SEM)

SEM effectively analyzes a sample's morphology using an electron microscope, which generates images with electrons instead of visible light. It is widely used due to its minimum sample preparation requirements and ease of use. Manfred von Ardenne designed the first

scanning electron microscope in 1937 [72]. SEM's spatial resolution ranges from 50 nm to 100 nm, with magnification levels between 20X and around 30,000X. Some SEMs can achieve even better than 1 nm resolution. The key components of SEM include an electron gun (source), lenses, an electron detector, and a sample chamber.

Working principle:

The operation of SEM involves focusing an electron beam onto the surface of a sample, where the electrons come into contact with the sample; they create secondary electrons, backscattered electrons, and characteristic X-rays. Detectors gather these emissions to produce high-resolution images and supply details about the sample's surface topography, composition, and other characteristics. In addition, Energy-dispersive X-ray analysis (EDAX or EDX) examines the elemental compositional analysis. This method utilizes X-ray analysis to determine the elemental composition of a material with a sensitivity of up to 0.5 - 1 atomic percent.

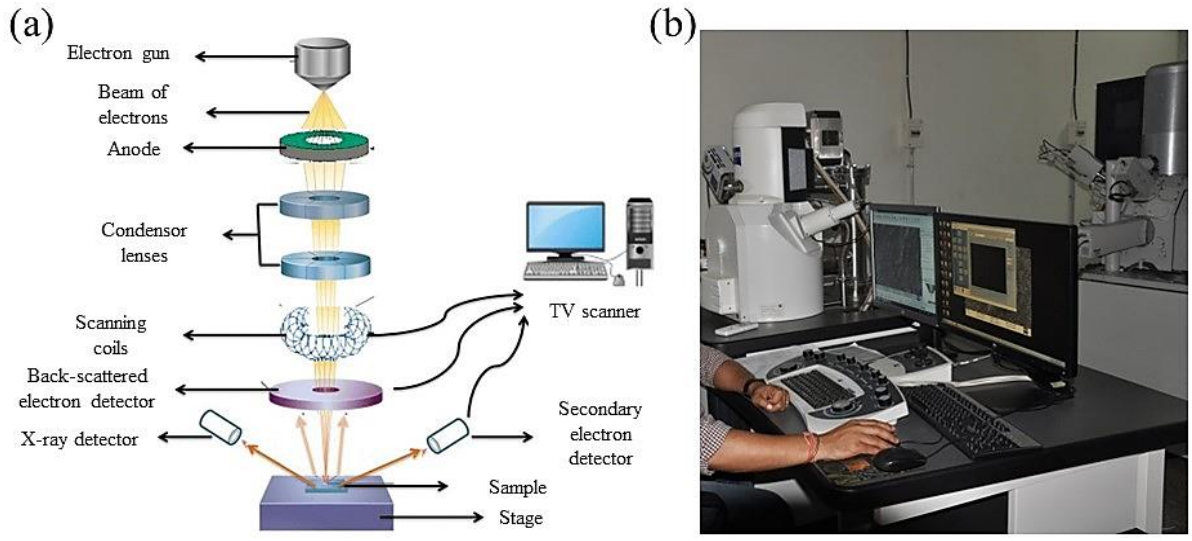

Figure 2.7: (a) Schematic representation of the working principle of SEM [73] (b) Experimental setup of SEM at CIF IIT(BHU).

The EDAX technique offers semi-quantitative and qualitative data about the elements in a given composition. In this thesis work, SEM and EDS data were obtained using the EVO - Scanning Electron Microscope MA15/18, as shown in Figure 2.7(b).

2.4.5 Transmission Electron Microscopy (TEM)

In 1931, two scientists, Max Knoll and Ernst Ruska, developed Transmission Electron Microscopy (TEM). It is an imaging technique that can visualize the internal structure of materials at atomic or molecular scales. Later, in 1986, Ernst Ruska was honored with the Nobel Prize in Physics for his contributions to electron optics and the development of electron microscopes. TEM employs a high-energy electron beam passed through an ultra-thin sample to create detailed images, allowing scientists to analyze the material's fine structure and properties.

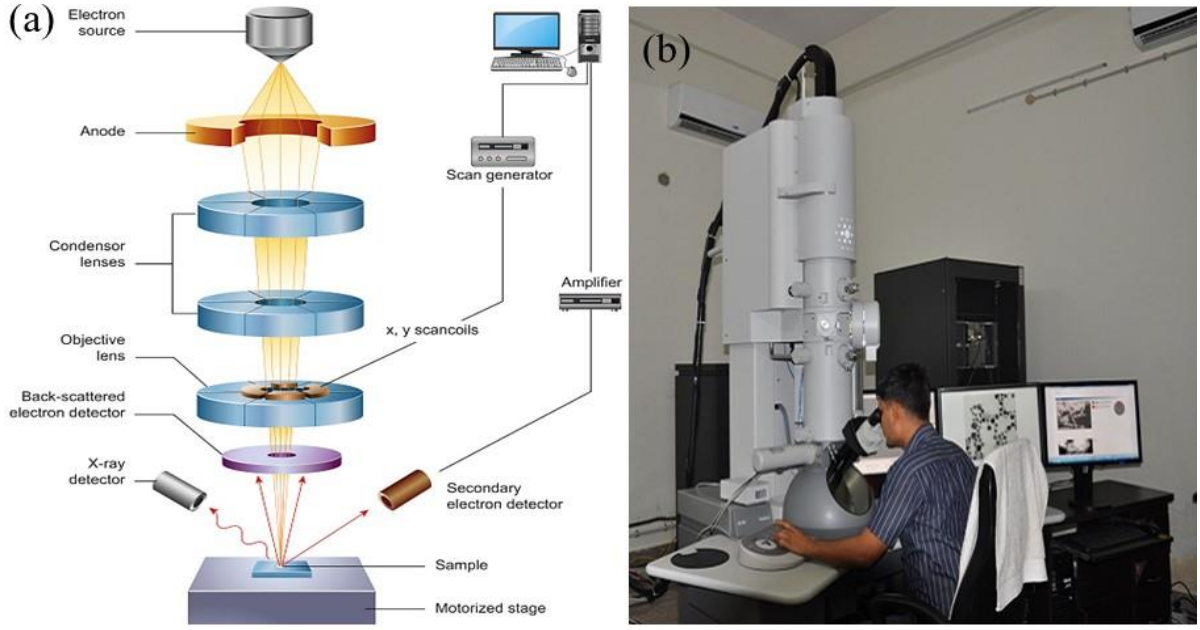

Figure 2.8: (a) Schematic representation of the working principle of TEM [74] (b) Experimental setup of TEM at CIF IIT (BHU).

Working principle:

In TEM, a beam of electrons penetrates an extremely thin sample. As the electrons pass through the sample, they interact with the atomic structures, causing them to scatter. Subsequently, the scattered electrons are focussed by a sequence of magnetic lenses to create an image on either a fluorescent screen or a digital detector. This method creates high-resolution images that unveil the internal structure and composition of the sample at an atomic scale. In this thesis work, TEM images were obtained using Tecnai G2 20 TWIN (FEI, USA), as shown in Fig. 2.8(b).

2.4.6 X-ray Photoelectron/Ultraviolet Photoelectron Spectroscopy (XPS/UPS)

X-ray Photoelectron Spectroscopy (XPS) and Ultraviolet Photoelectron Spectroscopy (UPS) are methods employed to examine the surface chemistry of materials [75]. XPS uses X-rays to eject core electrons from a sample, providing information about the elemental composition, chemical state, and electronic state of the elements in the surface layer. On the other hand, UPS utilizes ultraviolet light to displace valence electrons, providing insights into the material's surface's electronic structure and work function [76]. In 1887, XPS was discovered by Heinrich Rudolf Hertz, but he could not explain the photoelectric effect, and later it was explained by Albert Einstein in 1905. He describes a hypothesis that the energy carried by electromagnetic waves could only release in ‘packets’ of energy. Albert Einstein received a Nobel Prize in physics for his hypothesis in 1921.

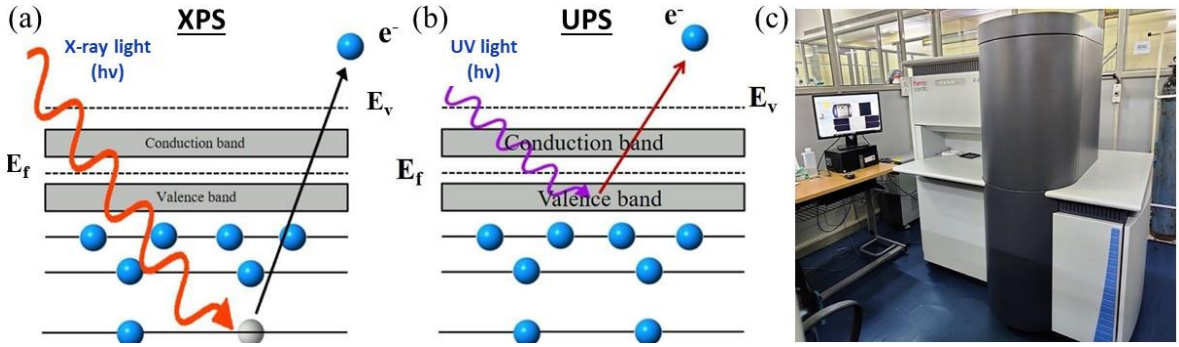

Figure 2.9: Schematic representation of the working principle of (a) XPS (b) UPS (c) Experimental setup of XPS/UPS at CIF IIT (BHU).

Working principle:

The working principle of XPS involves exposing the sample to X-rays, which remove core electrons from the atoms on the sample's surface, as shown in Fig. 2.9(a). The energy of these emitted electrons is measured to determine the binding energy. This data assists in identifying the elemental composition and chemical states on the surface. The electron binding energy (BE) and ionization (IE) energy can be written as [77]:

$$BE = h\nu - KE - \phi_{spec} \tag{2.4}$$

$$IE = h\nu - (E_{cutoff} - E_{VBM}) \tag{2.5}$$

where KE is the kinetic energy of the emitted electron and ϕ_{spec} represents the work function of a spectrometer, E_{cutoff} represents the secondary electron cutoff energy and E_{VBM} represents the energy of the valence band maximum relative to the Fermi level. Ultraviolet photoelectron spectroscopy (UPS) uses principles similar to XPS but utilizes lower-energy ultraviolet excitation rather than X-ray excitation, as shown in Fig. 2.9(b). Instead of stimulating core electrons, ultraviolet light causes transitions of the valence electrons, offering insights into the electronic structure of a semiconductor and the absolute energy of its valence band maximum.

In this thesis work, XPS and UPS images were obtained using K-Alpha (Thermo Fisher Scientific), as shown in Fig. 2.9(c).

2.4.7 Atomic Force Microscopy

In 1982, IBM research scientists discovered atomic force microscopy (AFM), a form of high-resolution scanning probe microscopy (SPM), also referred to as scanning force microscopy (SFM). This technique offers a resolution of fraction nanometers, which is significantly superior to the optical diffraction limit, by physically probing and "feeling" the sample's surface using a mechanical probe [78].

Working principle:

The AFM possesses three key capabilities: force measurement, imaging, and manipulation. In force measurement mode, it quantifies the force between the sample and the probe as their mutual separation changes. For imaging purposes, the forces exerted by the sample on the probe are used to generate high-resolution images of the three-dimensional (3D) shapes or topography of the sample's surface. Moreover, it can deliberately alter the properties of the sample by utilizing the forces between the sample and the probe.

The AFM process involves using a cantilever equipped with a sharp tip (probe) to scan the sample's surface. The cantilever is usually constructed from silicon or silicon nitride and features a tip with a nanometer-scale radius of curvature. As per Hooke's law, as the tip gets closer to the sample surface, the interaction between the tip and the sample causes cantilever deflection. There are three different types of modes of operation in AFM: (1) Contact mode, (2) Non-contact mode and (3) Tapping mode. Depending on specific circumstances, it can

detect various forces, such as mechanical contact, magnetic, capillary, chemical bonding, Van der Waals, and electrostatic forces.

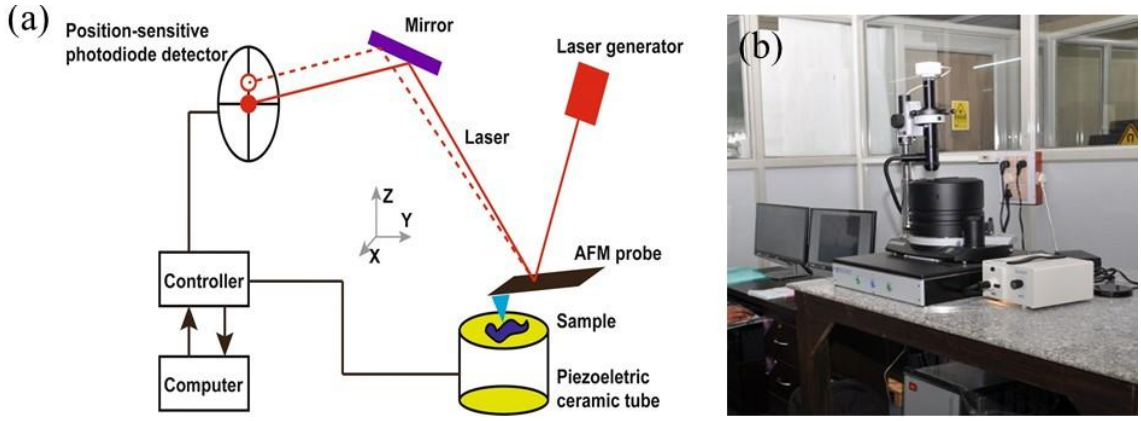

Figure 2.10: Schematic representation of (a) the working principle of AFM [79] and (b) the Experimental setup of AFM at CIF IIT (BHU).

The AFM is used in semiconductor technology, solid-state physics, polymer and chemistry, surface chemistry, molecular engineering, molecular biology, and medicine. The topography of thin-film samples synthesized in this thesis is recorded by the NTEGRA Prima (NT-MDT AFM instrument), as shown in Figure 2.10(b).

2.4.8 Ultraviolet-visible (UV - Vis) Spectroscopy

UV-Vis spectrometers have become the primary analytical instruments used to study the optical properties of materials because of their ease of use, quick results, flexibility, precision, and cost-effectiveness. UV-Vis spectroscopy allows examining sample absorption and reflection in the ultraviolet and visible spectral range. Furthermore, the UV-Vis data has been used to calculate the bandgaps of various samples, such as thin films, bulk powders, and liquids [80]. UV/Vis/NIR spectroscopy operates based on Beer-Lambert's law, which establishes a

linear correlation between the concentration and absorbance of the absorbing material. The following equation can express this law:

$$A = \log_{10}\left(\frac{I}{I_0}\right) = \varepsilon \times \ell \times c \qquad (2.3)$$

where A is absorbance, ε represents the wavelength-dependent absorptive coefficient, b is the path length, and c is the material concentration. Additionally, I_0 represents the intensity of the incident light, and I represent the intensity of the transmitted light. The spectrophotometer comprises four major components: the light source, the sample holder, the monochromator's diffraction grating, and the detector. The light source operates continuously for visible wavelengths, and the detector can be a charge-coupled device (CCD), photodiode, or photomultiplier tube. The monochromator is scanned using photomultiplier tubes and single photodiode detectors. It selectively transmits one wavelength at a time by filtering out all other wavelengths. By scanning the monochromator, each wavelength may be "step-through" transmitted using the diffraction grating, allowing the intensity of the light to be determined as a function of wavelength. In this thesis work, the JASCO V-770 ultraviolet-visible (UV) spectrometer has been used to record the optical absorption spectrum, as shown in Fig. 2.11(b). For the bandgap calculation of the samples, the Tauc equation has been used [81].

$$(\alpha h\nu)^{1/n} = A\left(h\nu - E_g\right) \qquad (2.4)$$

where E_g represents the optical bandgap, α represents the energy absorption coefficient, A represents the energy-independent constant, and hν represents incident photon energy, respectively. 'n' is the power factor of transition modes and is equal to 2 and ½ for the indirect and direct bandgap, respectively.

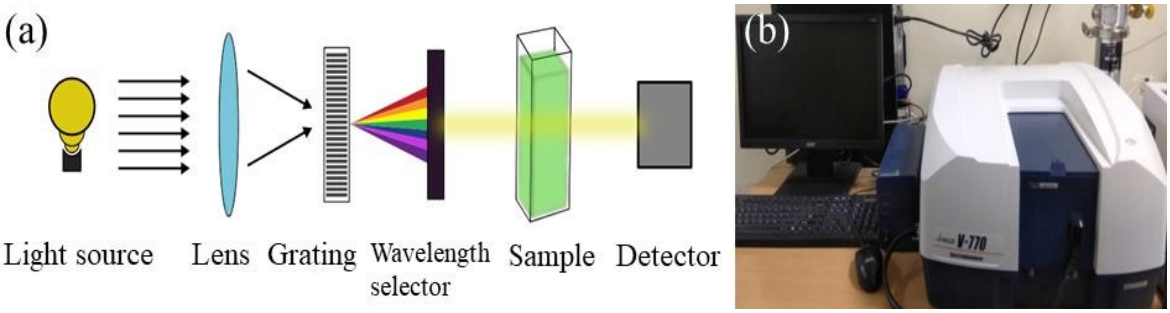

Figure 2.11: Schematic representation of (a) the working principle of UV-Vis spectrophotometer [82] and (b) the Experimental setup of UV-Vis at IIT (BHU).

2.4.9 Surface Enhanced Raman Spectroscopy (SERS)

Surface-enhanced Raman spectroscopy (SERS) is a highly sensitive analytical technique that amplifies the molecule's Raman scattering using nanostructured materials. By leveraging plasmon-induced electric field enhancement or chemical amplification, SERS enables detailed structural analysis of substances at low concentrations. Due to its exceptional sensitivity and selectivity, SERS is extensively applied across diverse areas, such as surface and interface chemistry, catalysis, nanotechnology, biology, biomedicine, food science, environmental analysis, and other fields. [83].

Working principle:

Raman spectroscopy depends on the inelastic scattering of photons, which is called Raman scattering. When a molecule interacts with light, the majority of photons are elastically scattered (Rayleigh scattering). Nevertheless, a small portion of the light undergoes inelastic scattering, leading to a shift in the wavelength of the scattered light. This shift provides information on the molecule's vibrational modes. In SERS, the Raman scattering gets enhanced by the factors of up to 10^6 to 10^{11}, making it possible to detect even a single molecule. In this

thesis work, the SERS imaging and Raman measurement were done using wavelength 532 nm by Witec Alpha RAS 300, Germany.

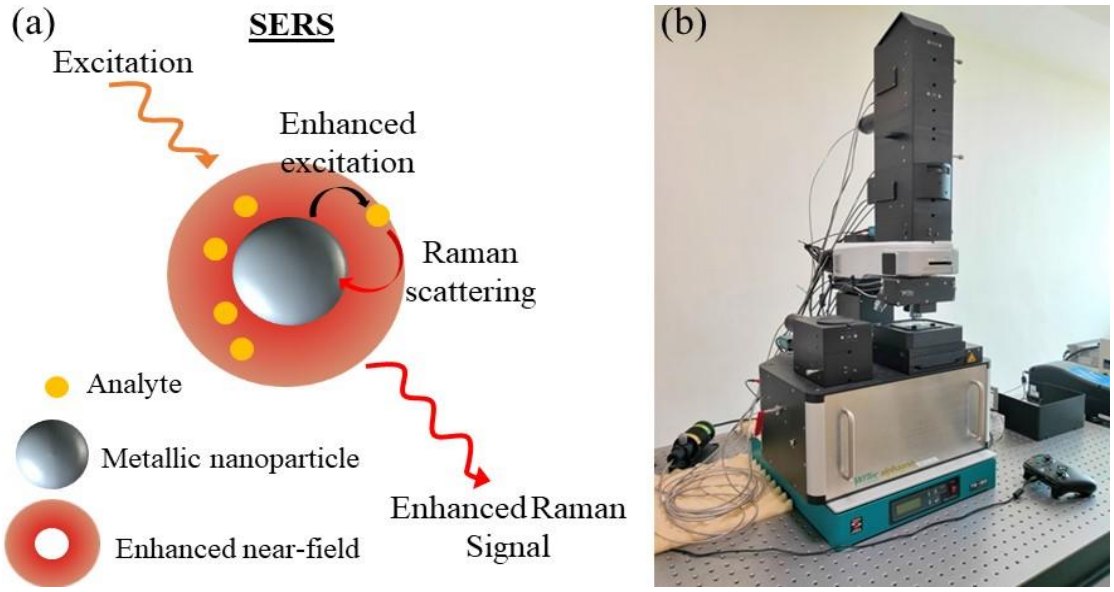

Figure 2.12: Schematic representation of (a) the working principle of SERS and (b) the Experimental setup of SERS at CDC BHU.

2.4.10 Cyclic Voltammetry (CV)

Cyclic voltammetry (CV) is a widely utilized electrochemical technique to study molecular specie's reduction and oxidation processes. It also investigates chemical reactions, such as catalysis driven by electron transfer. CV finds extensive application in HER, OER, and ORR, allowing the determination of reaction potential under different conditions. In 1938, Randles first provided a fundamental explanation of CV. Furthermore, it can provide qualitative and quantitative insights into electrochemical reactions, including their kinetics, reversibility, mechanisms, and other properties [84]. The Randles – Sevcik (RS) equation can be written as:

$$i_p = 0.446\, nFAC^0 \left(\frac{nF\nu D_0}{RT}\right)^{1/2} \qquad (2.5)$$

Figure 2.13: Schematic representation of (a) typical CV curve, (b) photoelectrochemical cell setup using CV at our laboratory, and (c) the CV setup.

where i_p is peak current, F is faraday constant, C^0 is the concentration, D_0 is diffusion coefficient, n is number of electrons, A is electrode surface area, R is gas constant, and T is temperature .Under various circumstances, such as when intermediate compounds are involved in oxidation-reduction reactions and when a reaction is reversible, cyclic voltammetry can provide qualitative insights into electrochemical processes. Cyclic voltammetry (CV) can also measure the analyte's diffusion coefficient and the system's electron stoichiometry. Moreover, a current versus concentration calibration curve can help estimate an unidentified solution's concentration [85][86].

Working principle:

Cyclic voltammetry (CV) operates by varying the electrode potential over time linearly in repetitive cycles. The resulting graph, a voltammogram or cyclic voltammogram, displays the applied potential on the x-axis and the resulting current on the y-axis. The scan rate (V/s) indicates how quickly the potential changes during each experiment phase. A three-electrode setup, consisting of a working electrode, counter electrode, reference electrode, and an electrolytic solution, is used for the measurement. The potential is measured between the

working and reference electrodes, while the current is determined between the working and counter electrodes. The electrodes are intended to accept ions from the electrolyte solution during the oxidation and reduction reactions. There will be no current flow at the initial potential, resulting in no peak on the voltammogram. As the potential increases and oxidized species are present, the anodic current (i_a) gradually increases until it reaches its maximum value (i_{pa}), indicating the oxidation of all species. Subsequently, (i_a) steadily decreases until it reaches the background current level. Upon reversing the potential, the oxidized species are then reduced. Consequently, (i_c) decreases until it reaches its maximum (i_{pc}), signifying the reduction of all species. Finally, (i_c) returns to the background level once again. The potential can be switched from negative to positive or vice versa, resulting in shifting the anodic and cathodic peak regions in the voltammogram. In the photoelectrochemical cell application, the CV setup includes solar radiation as an external source. This radiation significantly enhances electrochemical properties, such as efficient charge generation and separation and enhanced photocurrent density.

2.5 Analysis techniques

2.5.1 Rietveld Refinement Technique

X-ray diffraction (XRD) is the most widely used and impactful analytical method among the various available tools. R. M. Rietveld pioneered a technique for refining structure profiles using powder diffraction data from neutron radiation and X-rays. The Rietveld refinement method plays a crucial role in thoroughly examining the structural details of samples, effectively disentangling overlapping data and enabling an accurate structural assessment. Various parameters of these reflections, including their width, height, and position, can be

utilized to characterize multiple aspects of a material's structure. This technique uses least-squares refinement to determine the best match between the calculated and observed profiles. Rietveld refinement allows for the extraction of valuable information regarding the sample's structure. With monochromatic neutron sources, multiple factors create a Gaussian distribution. When considering this distribution, the impact of a particular reflection on the profile y_i at position $2\theta_i$ can be determined.

$$y_i = I_k \exp\left[\frac{-4\ln(2)}{H_k^2}(2\theta_i - 2\theta_k)^2\right] \quad (2.6)$$

where, H_k represents FWHM, $2\theta_k$ represents a reflex center and I_k represents the calculated intensity of the reflex (obtained from the Lorentz factor, the multiplicity of the reflection, and the structure factor), respectively. Reflection can acquire an asymmetry due to the vertical divergence of the beam at minimal diffraction angles. Rietveld applied a semi-empirical correction factor A_S to estimate this asymmetry.

$$A_S = 1 - \left[\frac{sP(2\theta_i - 2\theta_k)^2}{\tan\theta_k}\right] \quad (2.7)$$

At higher Bragg angles, the diffraction peak's width is wider. This angular dependency is formerly described by

$$H_k^2 = U\tan^2\theta_k + V\tan\theta_k + W \quad (2.8)$$

The Rietveld refinement process allows for the refinement of the half-width parameters U, V, and W. This technique evaluates the difference between the observed data (y_i^{obs}) and the calculated profile (y_i^{calc}), condensing it into the function M. This is given by:

$$M = \sum_i W_i \left\{ y_i^{obs} - \frac{1}{c} y_i^{calc} \right\}^2 \quad (2.9)$$

Here, c represents an overall scale factor, and W_i is the statistical weight, ensuring that $y^{calc} = c\, y^{obs}$. R-factors, also called residual factors, are the crucial parameters for the agreement between the crystallographic model and the experimental XRD data. The R-factors can be calculated from the following equations:

$$\text{Profile residual, } R_p = \sum_i^n \frac{|Y_i^{obs} - Y_i^{Calc}|}{\sum_i^n Y_i^{obs}} \times 100\% \quad (2.10)$$

$$\text{Weighted profile, } R_{wp} = \left(\sum_i^n \frac{w^i (Y_i^{obs} - Y_i^{Calc})^2}{\sum_i^n w^i (Y_i^{obs})^2} \right)^{1/2} \times 100\% \quad (2.11)$$

$$\text{Expected residual, } R_{exp} = \left(\frac{n-p}{\sum_i^n w^i (Y_i^{obs})^2} \right)^{1/2} \times 100\% \quad (2.12)$$

$$\text{Goodness of fit, } X^2 = \sum_i^n \frac{(Y_i^{obs} - Y_i^{calc})^2}{n-p} = \frac{(R_{wp})}{(R_{exp})} \quad (2.13)$$

The Fullprof Suite software is utilized in this thesis work to conduct the Rietveld refinement.

2.5.2 Software to Analyze the Obtained Data

In this thesis, Origin Pro software of the 2021 version was used to study the sample's electrical, structural, photoelectrochemical, and optical results. In addition, Image-J software was used to analyze the grain size distribution via SEM micrographs. Diamond 3.2 software has been used for the crystal structure of the synthesized samples.